

Nuclear collective dynamics within Vlasov approach

V. Baran¹, M. Colonna², M. Di Toro³, B. Frecus¹, A. Croitoru¹, D. Dumitru¹

¹ Faculty of Physics, University of Bucharest, Romania

² Laboratori Nazionali del Sud, INFN, I-95123 Catania, Italy

³ Physics and Astronomy Department, University of Catania, Italy

Received: date / Revised version: date

Abstract. We discuss, in an investigation based on Vlasov equation, the properties of the isovector modes in nuclear matter and atomic nuclei in relation with the symmetry energy. We obtain numerically the dipole response and determine the strength function for various systems, including a chain of Sn isotopes. We consider for the symmetry energy three parametrizations with density providing similar values at saturation but which manifest very different slopes around this point. In this way we can explore how the slope affects the collective response of finite nuclear systems. We focus first on the dipole polarizability and show that while the model is able to describe the expected mass dependence, $A^{5/3}$, it also demonstrates that this quantity is sensitive to the slope parameter of the symmetry energy. Then, by considering the Sn isotopic chain, we investigate the emergence of a collective mode, the Pygmy Dipole Resonance (PDR), when the number of neutrons in excess increases. We show that the total energy-weighted sum rule exhausted by this mode has a linear dependence with the square of isospin $I = (N - Z)/A$, again sensitive to the slope of the symmetry energy with density. Therefore the polarization effects in the isovector density have to play an important role in the dynamics of PDR. These results provide additional hints in the investigations aiming to extract the properties of symmetry energy below saturation.

PACS. PACS-key 21.65.Ef, 24.10.Cn, 24.30.Cz, 25.20.Dc

1 Introduction

After the early applications to the study of collisionless stellar dynamics [1] and in the context of plasma physics [2, 3], the Vlasov equation has also proved to be very useful in the investigation of the fermionic systems too, as are the atomic nuclei [4, 5, 6, 7], the electrons in atomic clusters [8, 9] or ultrafast electrons in thin metal films [10, 11]. For these quantum systems the Vlasov equation appears as a semiclassical limit of the quantum dynamics. In the field of nuclear physics, in many situations, the full quantum treatment is very involved and sometimes a clear physical picture can be difficult to extract. The passage to a semi-classical approach leads to simplifications and can provide a more transparent interpretation of the studied processes. Of course, the price to pay for this transition is the missing of important quantum correlations. However, as a reverse of the medal, such an approach may help to distinguish the role of various quantum effects. In the context of nuclear physics the quantum dynamics at the level of mean-field approximation is described by the time-dependent Hartree-Fock (TDHF) equation for the one-body density matrix ρ :

$$i\hbar \frac{d\rho}{dt} = [h_{MF}(\rho), \rho], \quad (1)$$

where $h_{MF}(\rho)$ is the single-particle Hartree-Fock Hamiltonian. Working with the density matrix in the position representation, $\rho_{\mathbf{r}'\mathbf{r}''}$, the Wigner transform defined as a kind of Fourier transform, is introduced:

$$f(\mathbf{r}, \mathbf{p}) \equiv \frac{1}{(2\pi\hbar)^3} \rho_{\text{Wigner}}(\mathbf{r}, \mathbf{p}) \\ = \frac{1}{(2\pi\hbar)^3} \int d^3s e^{-\frac{i}{\hbar}\mathbf{p}\cdot\mathbf{s}} \rho_{\mathbf{r}+\mathbf{s}/2, \mathbf{r}-\mathbf{s}/2}. \quad (2)$$

The exact equation satisfied by $f(\mathbf{r}, \mathbf{p}, t)$, equivalent with TDHF, is:

$$\frac{\partial f(\mathbf{r}, \mathbf{p}, t)}{\partial t} = \frac{2}{\hbar} \sin \frac{\hbar}{2} (\nabla_{\mathbf{r}_1} \nabla_{\mathbf{p}_2} - \nabla_{\mathbf{r}_2} \nabla_{\mathbf{p}_1}) \\ h(\mathbf{r}_1, \mathbf{p}_1) f(\mathbf{r}_2, \mathbf{p}_2, t) \Big|_{\substack{\mathbf{r}_1=\mathbf{r}_2=\mathbf{r} \\ \mathbf{p}_1=\mathbf{p}_2=\mathbf{p}}}. \quad (3)$$

where $h(\mathbf{r}, \mathbf{p})$ is the Wigner transformation of the $h_{MF}(\rho)$. This corresponds to a formulation of quantum mechanics in phase-space [12], where the dynamics is described in terms of Moyal brackets instead of Poisson brackets, and represents an appropriate starting point for modeling quantum plasmas [13]. In the limit $\hbar \rightarrow 0$, the Moyal bracket reduces to Poisson bracket and for a self-consistent mean-field approximated by a local one, we obtain the

Vlasov equation :

$$\frac{\partial f(\mathbf{r}, \mathbf{p}, t)}{\partial t} + \frac{\mathbf{p}}{m} \cdot \nabla_{\mathbf{r}} f(\mathbf{r}, \mathbf{p}, t) - \nabla_{\mathbf{r}} U(\mathbf{r}) \cdot \nabla_{\mathbf{p}} f(\mathbf{r}, \mathbf{p}, t) = 0. \quad (4)$$

In the semi-classical limit the quantum effects manifest through the Pauli correlations contained in the distribution function. These are included already from the initial conditions, since the Fermi-Dirac statistics should characterize the initial distribution of the fermions.

The purpose of this work is to describe recent applications of this equation to the study of collective features in two-components systems by focusing on some new properties of the Pygmy Dipole Resonance, a collective motion evidenced experimentally in nuclei with neutrons in excess. For a minimal self-consistency of the presentation, we shall start with a description of some known but fundamental results concerning the Vlasov dynamics in nuclear systems. This allows us to introduce the basic definitions and concepts required to characterize the nuclear systems and also will provide a reference for the results obtained later numerically. Then we describe the numerical implementation of the Vlasov equation to the nuclear dynamics and study in detail the dipole response by employing three different parametrization with density of the symmetry energy. We determine the strength function and investigate the mass and isospin dependence of the polarizability and of the sum-rule exhausted by PDR.

2 Isovector modes in nuclear matter

In the present section we describe the Vlasov approach to the collective dynamics of nuclear matter. This is a two component system and therefore the semi-classical dynamics is determined by two coupled Vlasov equations:

$$\frac{\partial f_p}{\partial t} + \frac{\mathbf{p}}{m} \cdot \nabla_{\mathbf{r}} f_p - \nabla_{\mathbf{r}} U_p \cdot \nabla_{\mathbf{p}} f_p = 0, \quad (5)$$

$$\frac{\partial f_n}{\partial t} + \frac{\mathbf{p}}{m} \cdot \nabla_{\mathbf{r}} f_n - \nabla_{\mathbf{r}} U_n \cdot \nabla_{\mathbf{p}} f_n = 0. \quad (6)$$

The nuclear mean-field contains an isoscalar as well as an isovector part and here we adopt a Skyrme-like (SKM^*) parametrization with nucleons density $\rho = \rho_n + \rho_p$:

$$U_q = A \frac{\rho}{\rho_0} + B \left(\frac{\rho}{\rho_0}\right)^{\alpha+1} + C(\rho) \frac{\rho_n - \rho_p}{\rho_0} \tau_q + \frac{1}{2} \frac{\partial C}{\partial \rho} \frac{(\rho_n - \rho_p)^2}{\rho_0} \quad (7)$$

Here $\rho_n(\mathbf{r})$ ($\rho_p(\mathbf{r})$) is the neutron (proton) local density and $\tau_n(\tau_p) = +1(-1)$. The saturation properties of the symmetric nuclear matter, the density $\rho_0 = 0.16 \text{ fm}^{-3}$, the binding energy $E/A = -16 \text{ MeV}$ and a compressibility modulus $K = 200 \text{ MeV}$, are reproduced with the values for the coefficients $A = -356 \text{ MeV}$, $B = 303 \text{ MeV}$, $\alpha = 1/6$. In the expression of total energy per particle,

$$\frac{E}{A}(\rho, I) = \frac{E}{A}(\rho) + \frac{E_{sym}}{A}(\rho) I^2 \quad (8)$$

the quantity depending on the isospin parameter $I = \frac{N-Z}{A}$, define the symmetry energy of the system. Since

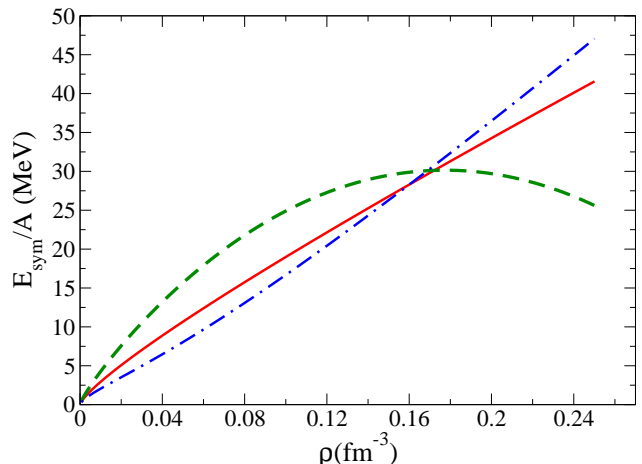


Fig. 1. (Color online) The density dependence of $\frac{E_{sym}}{A}$ for asystiff (dashed green line), asystiff (solid red line) and asysuperstiff (dot-dashed blue line).

the dipole response is determined by the symmetry energy term, containing both a kinetic and a potential contribution:

$$E_{sym}/A \equiv \epsilon_{sym} = \frac{E_F(\rho)}{3} + \frac{C(\rho)}{2} \frac{\rho}{\rho_0} \quad (9)$$

with E_F being the Fermi energy, we shall consider three different parametrizations with density of $C(\rho)$. We selected those parametrizations which provide quite similar values of E_{sym}/A at saturation but manifest very different slopes around this point, see Fig. 1. Specifically, for asystiff EOS, the coefficient $C(\rho)$ is constant, $C(\rho) = 32 \text{ MeV}$. Then the symmetry energy at saturation is $E_{sym}/A = 28.3 \text{ MeV}$ and the slope parameter $L = 3\rho_0 \frac{dE_{sym}/A}{d\rho} \Big|_{\rho=\rho_0}$ takes the value $L = 72 \text{ MeV}$. For the asysuperstiff EOS:

$$\frac{C(\rho)}{\rho_0} = (482 - 1638\rho) \text{ MeV fm}^3 \quad (10)$$

which leads to a quite small value of the slope parameter $L = 14.4 \text{ MeV}$. For the asysuperstiff EOS,

$$\frac{C(\rho)}{\rho_0} = \frac{32}{\rho_0} \frac{2\rho}{(\rho + \rho_0)} \quad (11)$$

the symmetry term has a faster variation around saturation density with a slope parameter $L = 96.6 \text{ MeV}$.

To study the collective modes of nuclear matter we consider small deviations of the distribution functions from equilibrium:

$$f_p(\mathbf{r}, \mathbf{p}, t) = f_p^0(E) + \delta f_p(\mathbf{r}, \mathbf{p}, t), \quad (12)$$

$$f_n(\mathbf{r}, \mathbf{p}, t) = f_n^0(E) + \delta f_n(\mathbf{r}, \mathbf{p}, t), \quad (13)$$

with $f_p^0(E) = f_n^0(E) = \frac{\gamma}{(2\pi\hbar)^3} \Theta(E - E_F)$ representing the equilibrium Fermi-Dirac distribution functions for

protons and neutrons and $\gamma = 2$. Within the linear approximation, the Eqs. (5),(6) become:

$$\frac{\partial \delta f_p}{\partial t} + \frac{\mathbf{p}}{m} \cdot \nabla_{\mathbf{r}} \delta f_p - \nabla_{\mathbf{r}} \delta U_p \cdot \nabla_{\mathbf{p}} f_p^0 = 0, \quad (14)$$

$$\frac{\partial \delta f_n}{\partial t} + \frac{\mathbf{p}}{m} \cdot \nabla_{\mathbf{r}} \delta f_n - \nabla_{\mathbf{r}} \delta U_n \cdot \nabla_{\mathbf{p}} f_n^0 = 0. \quad (15)$$

For the Skyrme-like parametrization of the mean-field potentials for protons and neutrons (see Eqs. (7)) one has:

$$\delta U_p = \frac{A}{\rho_0} (\delta \rho_n + \delta \rho_p) + \frac{B}{\rho_0} (\delta \rho_n + \delta \rho_p)^\sigma + \frac{C}{\rho_0} (\delta \rho_p - \delta \rho_n),$$

$$\delta U_n = \frac{A}{\rho_0} (\delta \rho_n + \delta \rho_p) + \frac{B}{\rho_0} (\delta \rho_n + \delta \rho_p)^\sigma + \frac{C}{\rho_0} (\delta \rho_n - \delta \rho_p).$$

Then the isovector variation $\delta f = \delta f_p - \delta f_n$, satisfy the equation:

$$\frac{\partial \delta f}{\partial t} + \frac{\mathbf{p}}{m} \cdot \nabla_{\mathbf{r}} \delta f - \nabla_{\mathbf{r}} (\delta U_p - \delta U_n) \cdot \left(-\frac{\mathbf{p}}{m} \delta(E - E_F) \right) = 0, \quad (16)$$

where

$$(\delta U_p - \delta U_n) = 2 \frac{C}{\rho_0} (\delta \rho_p - \delta \rho_n) = 2 \frac{C}{\rho_0} \int d^3 p \gamma \delta f. \quad (17)$$

Searching for a plane-wave solution:

$$\delta f(\mathbf{r}, \mathbf{p}, t) = \frac{\gamma}{(2\pi\hbar)^3} \sum_{\mathbf{k}} A_{\mathbf{k}}(\mathbf{p}) e^{i(\mathbf{k}\mathbf{r} - \omega t)}, \quad (18)$$

one can arrive, with $s = \frac{\omega}{k v_F}$, at the dispersion relation:

$$\frac{s}{2} \ln \frac{s+1}{s-1} - 1 = \frac{2 E_F}{3 C}. \quad (19)$$

The isovector collective mode velocity $\frac{\omega}{k}$ will depend now on the symmetry energy through the value of the parameter C . For $C = 32$ MeV the solution is $s = \frac{\omega}{k v_F} \approx 1.08$.

The isovector zero sound mode in nuclear matter is a quantum collective motion different from the hydrodynamical (or first sound) mode. While the first sound is driven by the pressure gradient, and so, requires the local thermodynamical equilibrium, the zero sound is determined by the mean-field and therefore propagates even at $T = 0$ MeV. In finite nuclei, this isovector zero sound mode will correspond to the Giant Dipole Resonance. Considering a wave-number k determined by the size of the Tin isotope ^{132}Sn , the energy of the GDR phonon would be expected around $\hbar\omega \approx 15$ MeV, quite close to the experimental results. In the next section we investigate numerically the dynamics of this mode in finite systems and study its evolution with the number of excess neutrons $N - Z$ by considering a chain of Sn isotopes, $^{108,116,124,132,140,148}\text{Sn}$.

We would like complete this general presentation mentioning that similar investigations can be extended to the study of instabilities in nuclear matter [14]. Moreover, if the present treatment is completed by adding a collision term in the relaxation time approximation, the nature of the zero to first sound transition in binary Fermi liquids can be explored [15,16].

3 Giant and Pygmy Dipole Resonances in neutron rich nuclei

3.1 Numerical implementation and static properties

The essential task of the transport approach based on Vlasov equation is to provide the value of the one-body distribution function at any time. Once this quantity is known, the expectation values of any one-body observable, $A(\mathbf{r}, \mathbf{p})$, can be evaluated as an integral over phase-space. In particular, the total number of protons, Z , is:

$$Z = \int d^3 r d^3 p f_p(\mathbf{r}, \mathbf{p}, t). \quad (20)$$

The numerical approach employed in our work is based on test particle method. This method starts from the observation that the Gaussian functions generate, as coherent states, a super-complete basis. Then, the following expansion for the distribution function is valid:

$$f(\mathbf{r}, \mathbf{p}, t) = \frac{1}{(2\pi\hbar)^3} \int d^3 r_0 d^3 p_0 \omega(\mathbf{r}_0, \mathbf{p}_0, 0) g(\mathbf{r} - \mathbf{r}_0, \mathbf{p} - \mathbf{p}_0, t), \quad (21)$$

where $g(\mathbf{r} - \mathbf{r}_0, \mathbf{p} - \mathbf{p}_0, t)$ corresponds to a product of Gaussian functions in coordinate and momentum space, centered in \mathbf{r}_0 and \mathbf{p}_0 respectively, while $\omega(\mathbf{r}_0, \mathbf{p}_0, 0)$ represents the corresponding weight in the expansion of g . In our numerical implementation, this expansion is discretized into a sum over a sufficiently large number of Gaussian functions [17,18]:

$$f(\mathbf{r}, \mathbf{p}, t) = \frac{1}{\mathcal{N}} \frac{1}{(2\pi\hbar)^3} \frac{1}{(4\pi^2\chi\phi)^{3/2}} \sum_i^N \exp\left(-\frac{(\mathbf{r} - \mathbf{r}_i(t))^2}{2\chi}\right) \exp\left(-\frac{(\mathbf{p} - \mathbf{p}_i(t))^2}{2\phi}\right). \quad (22)$$

Here $\mathbf{r}_i(t)$ and $\mathbf{p}_i(t)$ define the centroid positions in coordinates and momentum space of the i -Gaussian function, which corresponds to an individual test particle. \mathcal{N} indicates the number of test particles per nucleon. The total number of test particles will be $N_{tot} = A \cdot \mathcal{N}$ and its value is limited by the requirement to have a reasonable computational effort. From a comparison with the particle-in-cell (PIC) simulation method employed in plasma dynamics [3], we observe that while in a present treatment several "test particles" are ascribed to a real particle, in order to obtain a very good spanning of phase-space and reduce the numerical fluctuations, in the PIC approach can be considered "finite size superparticles" which will incorporate several real particles, reducing so the numerical effort, in such a way that charge density, the mass density and the thermal energy density match the same values as those of the real particles and the same long-range behavior as in real plasma is maintained [19]. The Gaussian functions which appear in Eq. (22) are normalized as follows:

$$g_\chi(\mathbf{r} - \mathbf{r}_i) = \frac{1}{(2\pi\chi)^{3/2}} \exp\left(-\frac{(\mathbf{r} - \mathbf{r}_i)^2}{2\chi}\right), \quad (23)$$

$$g_\phi(\mathbf{p} - \mathbf{p}_i) = \frac{1}{(2\pi\phi)^{3/2}} \exp\left(-\frac{(\mathbf{p} - \mathbf{p}_i)^2}{2\phi}\right), \quad (24)$$

so that one has:

$$\int d^3r g_\chi(\mathbf{r} - \mathbf{r}_i) = 1; \int d^3p g_\phi(\mathbf{p} - \mathbf{p}_i) = 1. \quad (25)$$

Substituting these expressions into the Vlasov equation (Eq. (4)), we find that the centroids of each Gaussian, \mathbf{r}_i and \mathbf{p}_i must satisfy Hamilton equations, that is:

$$\frac{\partial \mathbf{r}_i}{\partial t} = \frac{\mathbf{p}_i}{m}, \quad (26)$$

$$\frac{\partial \mathbf{p}_i}{\partial t} = -\nabla_{\mathbf{r}_i} U(\mathbf{r}_i). \quad (27)$$

More generally, the average value of an arbitrary physical quantity, $A(\mathbf{r}, \mathbf{p})$, can be expressed:

$$\begin{aligned} \langle A(\mathbf{r}, \mathbf{p}) \rangle &= \int d^3r d^3p A(\mathbf{r}, \mathbf{p}) f(\mathbf{r}, \mathbf{p}, t) \\ &= \frac{1}{N} \frac{1}{(2\pi\hbar)^3} \sum_i^N \int d^3r d^3p A(\mathbf{r}, \mathbf{p}) g_\chi(\mathbf{r} - \mathbf{r}_i) g_\phi(\mathbf{p} - \mathbf{p}_i) \\ &= \frac{1}{N} \frac{1}{(2\pi\hbar)^3} \sum_i^N \langle A(\mathbf{r}, \mathbf{p}) \rangle_i, \end{aligned} \quad (28)$$

where $\langle A(\mathbf{r}, \mathbf{p}) \rangle_i$ represents the contribution of an individual Gaussian. This contribution is obtained by the convolution of A with the corresponding Gaussians in coordinate and momentum space:

$$\langle A(\mathbf{r}, \mathbf{p}) \rangle_i = \int d^3r d^3p A(\mathbf{r}, \mathbf{p}) g_\chi(\mathbf{r} - \mathbf{r}_i(t)) g_\phi(\mathbf{p} - \mathbf{p}_i(t)). \quad (29)$$

The method described above can reproduce accurately the equation of state of the nuclear matter as well as the properties of the nuclear surface [20] and the ground state energy for finite nuclei [18]. Here we discuss the predictions concerning the neutron skin of the Sn isotopic chain when a number of 1300 t.p. per nucleon is adopted. From the one-body distribution functions one obtains the local densities: $\rho_q(\mathbf{r}, t) = \int 2d^3p f_q(\mathbf{r}, \mathbf{p}, t)$ as well as the quadratic radii $\langle r_q^2 \rangle = \frac{1}{N_q} \int r^2 \rho_q(\mathbf{r}, t) d^3\mathbf{r}$ and the width

of the neutrons skin $\Delta R_{np} = \sqrt{\langle r_n^2 \rangle} - \sqrt{\langle r_p^2 \rangle} = R_n - R_p$.

A possible method to obtain R_n and R_p is by observing their time evolution after a weak monopolar perturbation. Both quantities perform small oscillations around equilibrium values and we remark that the numerical simulations keep a very good stability of the dynamics for at least $1800 fm/c$ [21]. Using this procedure we obtain for the charge mean square radius of ^{208}Pb a value around $R_p = 5.45 fm$, to be compared with the experimental value $R_{p,exp} = 5.50 fm$. Analogously for ^{124}Sn we obtain $R_p = 4.59 fm$ while experimentally $R_{p,exp} = 4.67 fm$. For Sn isotopes and asystiff EOS we display the isospin parameter $I = \frac{N-Z}{A}$ dependence of ΔR_{np} respectively in Fig. 2.

3.2 Collective dipole response: the emergence of Pygmy Dipole Resonance

We explore in this section, for various nuclear systems, some new the features of the E1 response in the Vlasov

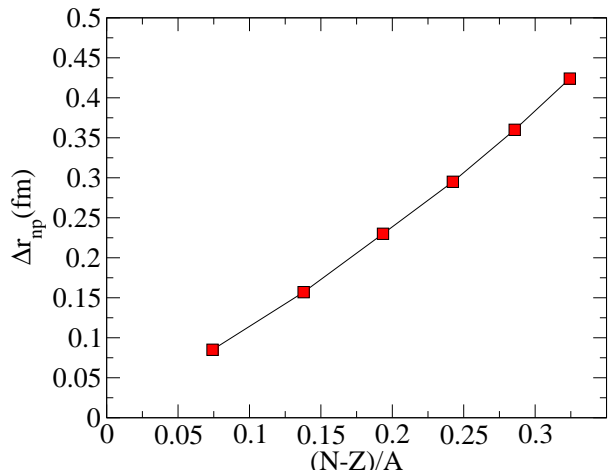


Fig. 2. (Color online) The neutron skin thickness as a function of $I = \frac{N-Z}{A}$ for $^{108,116,124,132,140,148}Sn$ isotopes. Asystiff EOS.

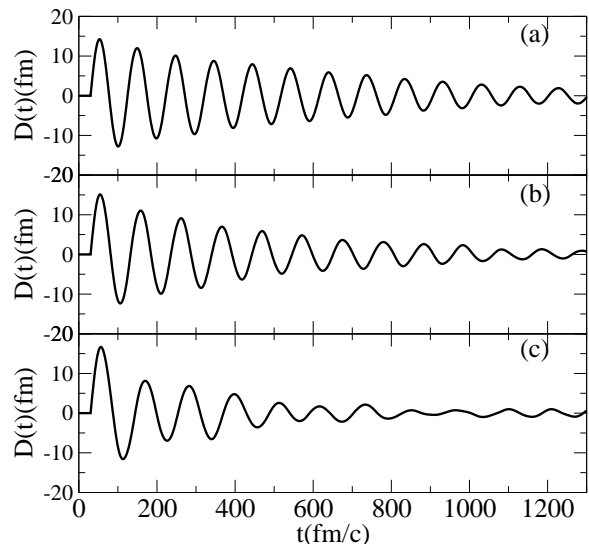


Fig. 3. The time evolution of the dipole moment following a GDR-like initial condition for (a) ^{108}Sn , (b) ^{124}Sn and (c) ^{148}Sn . Asystiff EOS.

approach. We consider a GDR-like initial condition [22] which corresponds to a boost of all neutrons against all protons while keeping the Center of Mass (CM) at rest. This is described by the instantaneous excitation $V_{ext} = \eta \delta(t - t_0) \hat{D}$ at $t = t_0$ [8]. If $|\Phi_0\rangle$ is the state before perturbation then the excited state becomes $|\Phi(t_0)\rangle = e^{i\eta \hat{D}} |\Phi_0\rangle$, where \hat{D} is the dipole operator. The value of η can be related to the initial expectation value of the collective dipole momentum $\hat{\Pi}$:

$$\langle \Phi(t_0) | \hat{\Pi} | \Phi(t_0) \rangle = \hbar \eta \frac{NZ}{A}. \quad (30)$$

If the collective coordinate which defines the distance between the CM of protons and the CM of neutrons is \hat{X} ,

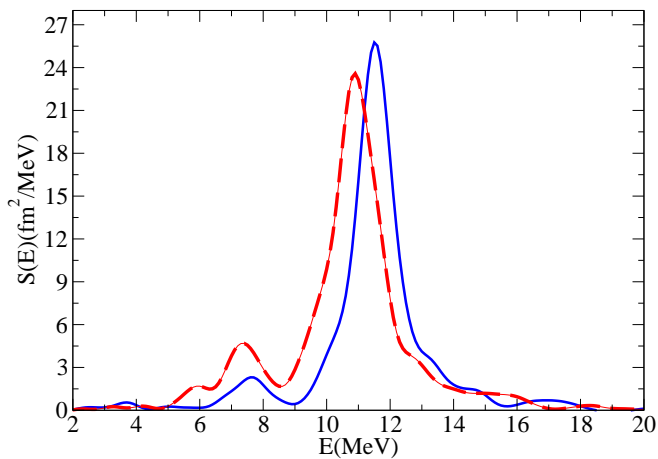


Fig. 4. (Color online) The strength function for ^{132}Sn [the blue (solid) lines] and ^{148}Sn [the red (dashed) lines]. Asystiff EOS.

then $\hat{\Pi}$ is canonically conjugated momentum, i.e. $[\hat{X}, \hat{\Pi}] = i\hbar$ [23]. We determine semi-classically the strength function:

$$S(E) = \sum_{n>0} |\langle n|\hat{D}|0\rangle|^2 \delta(E - (E_n - E_0)), \quad (31)$$

where E_n are the excitation energies of the states $|n\rangle$ while E_0 is the energy of the ground state $|0\rangle = |\Phi_0\rangle$. In our approach this is obtained from the imaginary part of the Fourier transform of the time-dependent expectation value of the dipole momentum $D(t) = \frac{NZ}{A} X(t) = \langle \Phi(t)|\hat{D}|\Phi(t)\rangle$ extracted from our simulations (see Fig. 3). We have:

$$S(E) = \frac{\text{Im}(D(\omega))}{\pi\eta\hbar}, \quad (32)$$

where $D(\omega) = \int_{t_0}^{t_{max}} D(t)e^{i\omega t} dt$. We consider the initial perturbation along the z -axis and integrate numerically the Vlasov equations (5, 6) until $t_{max} = 1830 fm/c$. η was determined from the numerical value of the collective momentum at $t = t_0 = 30 fm/c$. In order to eliminate the artifacts resulting from a finite time domain analysis of the signal a filtering procedure, as described in [24], was considered. A smooth cut-off function was introduced such that $D(t) \rightarrow D(t)\cos^2(\frac{\pi t}{2t_{max}})$. The E1 strength functions of ^{132}Sn and ^{148}Sn are represented in Fig. 32. A test of the quality of our method is the comparison of the numerically estimated value of the first moment $m_1 = \int_0^\infty ES(E)dE$ with the value predicted by the

Thomas-Reiche-Kuhn (TRK) sum rule $m_1 = \frac{\hbar^2}{2m} \frac{NZ}{A}$. In all cases the difference was below 5%.

Before discussing the dipole response below GDR region let us observe that from the strength function one

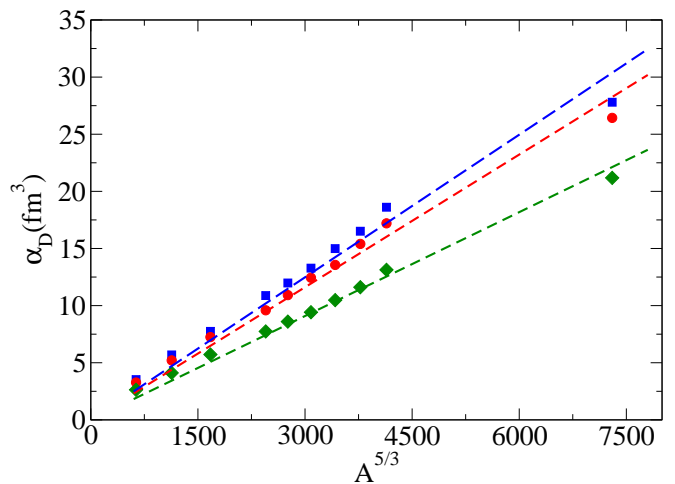


Fig. 5. (Color online) The dipole polarizability as a function of $A^{5/3}$ for asysuperstiff (blue squares) asystiff (red circles) and asysoft (green diamonds) EOS. The corresponding dashed lines provide the best linear fit of α_D with $A^{5/3}$. The correlation coefficients r_{fit} are 97%, 98% and 99% respectively.

can determine the nuclear dipole polarizability:

$$\alpha_D = 2e^2 \int_0^\infty \frac{S(E)}{E} dE. \quad (33)$$

For ^{68}Ni the experimental value of α_D reported recently, [26] is $3.14 fm^3$ while we obtained values from $4.1 fm^3$ from $5.7 fm^3$ when we pass from asysoft to asysuperstiff EOS [21]. In the case of ^{208}Pb the experimental value of α_D is around $20.1 fm^3$ [27]. In our approach it changes from $21.1 fm^3$ for asysoft EOS to $28.6 fm^3$ for asysuperstiff. Here we want to explore the mass dependence of this quantity for the three asy-EOS. In order to accomplish this goal we consider the systems ^{48}Ca , ^{68}Ni , ^{86}Kr , ^{208}Pb as well as the mentioned isotopic chain of Sn. The Migdal estimation of polarizability [28], valid for large systems, provides a $A^{5/3}$ dependence with mass:

$$\alpha_D = \frac{e^2 A \langle r^2 \rangle}{24\epsilon_{sym}} = \frac{1.44e^2}{40\epsilon_{sym}} A^{\frac{5}{3}}, \quad (34)$$

considering that $\langle r^2 \rangle = \frac{3}{5} R^2$ and $R = 1.2A^{\frac{1}{3}}$. Since ϵ_{sym} , at saturation, has similar values for the three asy-EOS one also expect, in this situation, close values for the polarizability. In Fig. 5 we show the polarizability α_D as a function of $A^{5/3}$. The linear correlation is quite well verified. Nevertheless a clear dependence of the slope with asy-EOS is evidenced. This can be related to the surface effects and the interplay between surface and volume symmetry energy, expected to manifest in finite systems [29] and which will be influenced by the symmetry energy slope parameter L .

Returning to the strength function, one can identify the appearance of a resonant response below GDR, more important when the number of neutrons in excess is larger.

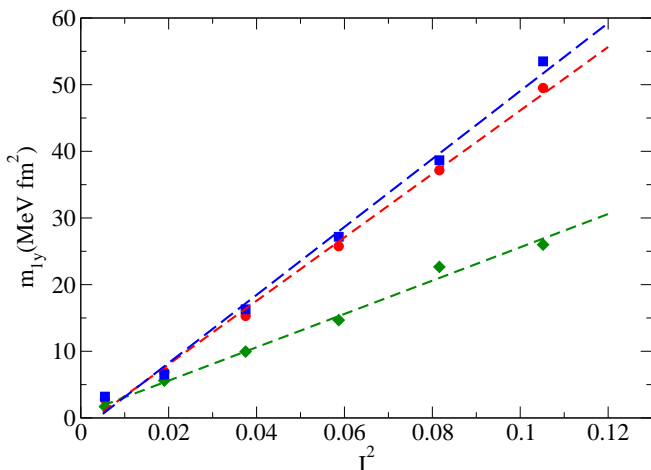


Fig. 6. (Color online) The EWSR exhausted by PDR as a function of I square, for asuperstiff (blue squares), asystiff (red circles) and asysoft (green diamonds) EOS. Were considered the systems ^{108}Sn , ^{116}Sn , ^{124}Sn , ^{132}Sn , ^{140}Sn and ^{148}Sn . The dashed lines correspond to the best fit of $m_{1,y}$ with I^2 . The correlation coefficients r_{fit} are 99.3%, 99.6% and 99.1% respectively.

In the present model the energy centroid is very well described by the parametrization $41A^{-\frac{1}{3}}$ [21], in nice agreement with several experimental data. This new mode we associate with Pygmy Dipole Resonance (PDR) and notice that other studies based on Vlasov equations arrived at similar conclusions [22,23,25,30]. Here our purpose is to investigate the dependence of PDR response on the isospin parameter I . We calculate EWSR exhausted by this mode by integrating over the low-energy resonance region:

$$m_{1,y} = \int_{PDR} ES(E)dE . \quad (35)$$

and plot its dependence on $I = \frac{N-Z}{A}$ in Fig. 6. From our calculations, for Sn isotopes, a quadratic correlation appears to describe quite well the observed dependence of $m_{1,y}$ with the isospin parameter I . We remark that, as in the case of polarization, the linear correlation between $m_{1,y}$ and I^2 is influenced by the symmetry energy slope parameter L . We can therefore conclude that polarization effects in the isovector density play an important role in the dynamics of Pygmy Dipole Resonance.

The PDR was observed experimentally for several systems [31,32] and discussed in different theoretical models [33] for various nuclei, including the Sn isotopic chain [34,35,36,37,38]. Concerning the features of this mode, in literature still exists an intense debate about the collective character of this mode, about the role of symmetry energy as well as about its isovector/isoscalar structure. While the relativistic quasiparticle RPA (RQRPA) [39,40] provides evidences about collectivity of PDR, from amplitudes and transition matrix elements, the nonrelativistic Hartree-Fock-Bogoliubov treatment within quasiparticle-phonon model [41], assign to the resonant structures non-

collective properties. The calculations based on relativistic time-blocking [42] also shows in the dipole spectra of even-even ^{130}Sn - ^{140}Sn nuclei two well separated collective structures, the lower lying one, having a specific behavior of the transition densities of states, being ascribed to PDR. For ^{34}Mg , from the time-dependent density plots obtained within TDHF calculations with Skyrme interaction, was identified a superimposed surface mode, not fully coupled to the bulk dynamics. This was related to the pygmy-like peak, obtained around 10 MeV, in the dipole response strength [43].

4 Conclusions

Summarizing, the main task in this paper was to present new results regarding the collective dipole response in connection with the properties of the symmetry energy below saturation. Our investigation was performed in a microscopic transport model based on a system of two coupled Vlasov equations for protons and neutrons.

For all studied asy-EOS our model predicts that the energy weighted sum-rule exhausted by the Pygmy Dipole Resonance manifests a linear dependence with the square of isospin parameter $I = (N-Z)/A$, with a slope which is influenced by the variation rate with density of the symmetry energy around saturation. Even if were considered asy-EOS providing similar values of symmetry energy at saturation was also observed that the slope of dipole polarizability as a function of $A^{5/3}$ changes with the symmetry energy slope parameter L . We interpret these results as an indication of the surface effects associated to the polarization of isovector density in finite nuclei.

In conclusion, the models based on Vlasov equation prove to be appropriate tools for the study of several aspects of nuclear dynamics, including the development of quite feeble modes as is Pygmy Dipole Resonance, for which provides qualitative insights but also quantitative information regarding its dependence on the symmetry energy or its evolution with the isospin parameter and mass number.

5 Acknowledgments

This work for V. Baran and A. Croitoru was supported by a grant of the Romanian National Authority for Scientific Research, CNCS - UEFISCDI, project number PN-II-ID-PCE-2011-3-0972.

References

1. J.H. Jeans, Monthly Notices Roy. Astron. Soc. **76**, (1913) 71.
2. A.A. Vlasov, Zh. Eksp. i Teor. Fiz. **8**, (1938) 291.
3. C.K. Birdsall and A.B. Langdon, *Plasma Physics via Computer Simulations*, Taylor and Francis, 1991.
4. D.M. Brink, M. Di Toro, Nucl. Phys. **A 372**, (1981) 151.

5. G.F. Bertsch and S. Das Gupta, Phys. Rep. **160**, (1988) 189.
6. A. Bonasera, F. Gulminelli, J. Molitoris, Phys. Rep. **243**, (1994) 1.
7. V. Baran, M. Colonna, M. Di Toro, V. Greco, Phys. Rep. **410**, (2005) 335.
8. F. Calvayrac, P.G. Reinhard, E. Suraud, Ann. Phys. **225**, (1997) 125.
9. Th. Fennel et al., Rev. Mod. Phys. **82**, (2010) 1793.
10. G. Manfredi, P.A. Hervieux, Phys. Rev. **B 70**, (2004) 201402.
11. N. Crouseilles, P.A. Hervieux, G. Manfredi, Phys. Rev. **B 78**, (2008) 155412.
12. J.E. Moyal, Proc. Cambridge Phil. Soc. **45**, (1949) 99.
13. G. Manfredi, Fields Inst. Commun. **46**, (2005) 263.
14. V. Baran, M. Colonna, M. Di Toro, V. Greco, Phys. Rev. Lett. **86**, (2001) 4492.
15. A.B. Larionov, M. Cabibbo, V. Baran, M. Di Toro, Nucl. Phys. **A 648**, (1999) 157.
16. V. Baran, M. Colonna, M. Di Toro, A.B. Larionov, Nucl. Phys. **A 649**, (1999) 185C; 6th International Topical Conference on Giant Resonances, Varenna, Italy, (1998).
17. C. Gregoire et al., Nucl. Phys. **A 465**, (1987) 77.
18. P. Schuck et al., Prog. Part. Nucl. Phys. **22**, (1989) L81.
19. A.B. Langdon, C.K. Birdsall, The Physics of Fluids **13**, (1970) 2115.
20. D. Idier, B. Benhassine, M. Farine, B. Remaud, F. Sebillie, Nucl. Phys. **A 564**, (1993) 204.
21. V. Baran, M. Colonna, M. Di Toro, A. Croitoru, D. Dumitru, Phys. Rev. **C 88**, (2013) 044610.
22. V. Baran, B. Frecus, M. Colonna, M. Di Toro, Phys. Rev. **C 85**, (2012) 051601.
23. V. Baran et al., Rom. J. Phys. **57**, 36 (2012).
24. P.-G. Reinhard, P.D. Stevenson, D. Almeded, J.A. Maruhn, M.R. Strayer, Phys. Rev. **E 73**, 036709 (2006).
25. V.I. Abrosimov, O.I. Davydov's'ka, Ukr. J. Phys. **54**, 1068 (2009).
26. D. M. Rossi et al., Phys. Rev. Lett. **111**, (2013) 242503.
27. A. Tamii et al., Phys. Rev. Lett. **107**, (2011) 062502.
28. A. Migdal, J. Phys. **8**, (1944) 331.
29. E. Lipparini, S. Stringari, Phys. Lett. **B 112** (1982) 421.
30. M. Urban, Phys. Rev. **C 85**, 034322 (2012).
31. T. Aumann and T. Nakamura, Phys. Scr. **T 152**, 014012 (2013).
32. D. Savran, T. Aumann and A. Zilges, Prog. Part. Nucl. Phys. **70**, (2013) 210 .
33. N. Paar, J. Phys. G: Nucl. Part. Phys. **37**, (2010) 064014.
34. N. Paar, T. Niksic ,D. Vretenar, P. Ring, Phys. Lett. **B 606** (2005) 288.
35. N. Tsoneva, H. Lenske, Phys. Rev. **C 77** (2008) 024321.
36. D.P. Arteaga, E. Khan, P. Ring, Phys. Rev. **C 79** (2009) 034311.
37. I. Daoutidis, S. Goriely, Phys. Rev. **C 86** (2012) 034328.
38. P. Papakonstantinou, H. Hergert, V. Yu. Ponomarev, R.Roth, Phys. Rev. **C 89** (2014) 034306.
39. N. Paar, D. Vretenar, E. Khan, G. Colo, Rep. Prog. Phys. **70**, (2007) 691.
40. N. Paar, Y.F. Niu, D. Vretenar, J. Meng, Phys. Rev. Lett. **103**, (2009) 032502.
41. N. Tsoneva, H. Lenske, Ch. Stoyanov, Phys. Lett. **B 586** (2004) 213.
42. E. Litvinova, P. Ring, V. Tselyaev, K. Langanke, Phys. Rev. **C 79**, (2009) 054312.
43. M.P. Brine, P.D. Stevenson, J.A. Mahrun, P.-G. Reinhard, Int. J. Mod. Phys. **E 15** (2006) 1417.